Application of Recurrence Quantification Analysis to Electrostatic Measurements of Horizontal Gas-solid Flow in Pneumatic Conveying of Plastic Pellets

Osamh S. Alshahed[1], Baldeep Kaur[1], Michael S.A. Bradley[1]

[1]The Wolfson Centre for Bulk Solids Handling Technology, University of Greenwich, Central Avenue, Chatham Maritime, Kent, ME4 4TB, United Kingdom

ABSTRACT The recurring dynamics of fully developed gas-solid flow patterns are characterised using recurrence quantification analysis of bottom arch-shaped electrostatic sensor data in horizontal pneumatic conveying of plastic pellets. The recurrence quantification analysis is applied to recurrence plots developed from phase spaces (attractors) reconstructed from the bottom arc-shaped electrostatic sensor signals using a statistical measure, the approximate entropy (AE). The AE measure is the probability of the unpredictability between past and future dynamics in a phase space used to select a specific range of recurring dynamics in the recurrence plot to characterise different flow patterns: stratified flow, pulsating flow, moving dunes and blowing dunes. The flow patterns were identified using high-speed video imaging of a transparent pipeline and classified at several operating conditions in a flow pattern map and state diagram. It is found that optimal operating conditions at the minimum energy consumption conveying operation in the state diagram are between moving dunes and blowing dunes. Through visual observation, recurrence plots of the identified flow patterns showed different qualitative structures. The qualitative structure of recurrence plots is quantified using a recurrence quantification analysis measure, the recurrence rate (RR). The AE and RR measures are correlated with the state diagram, indicating that the complexity of electrostatic sensor signals can classify the flow patterns at different operating conditions.

1. INTRODUCTION

There are three main modes of operation in horizontal pneumatic conveying of particulate materials, dilute phase, transition phase and dense phase. Choosing between these phases during conveying can be challenging depending on the material properties, conveying route structure and distance, and pressure availability in the pipelines. Dilute phase flow operation is considered when a simple pneumatic conveying system design is required to achieve a stable and reliable operation [1]. Dilute phase flow operates at a high air velocity in large volumes and low solids concentrations, where discrete solid particles are uniformly suspended via drag and lift forces caused by turbulent air stream [2]. In practice, pneumatically conveying solids at high air velocity often result in high energy consumption, material degradation and pipeline wear [3]. Dense phase flow operation is characterised by a high concentration of particles and low air velocity, resulting in improved product quality and reduced pipeline sizing and wear rate [4]. However, the dense phase flow operation requires more pressure availability resulting in a high initial cost of equipment to withstand high-pressure operations. Particulate materials with dense phase operation capability, such as coarse plastic pellets with a mean diameter higher than 1 mm [20], operating in the transition phase between the dilute and dense phase, will reduce energy consumption and pipeline wear and improve product quality.

The flow pattern map and the state diagram are common ways of describing the gas-solid flow transition spectrum from dilute to dense phase flow operations for specific particulate material. The flow pattern map shows a distribution of operating condition points, including air and solids mass flow rates, classified according to the observed flow patterns in a transparent pipeline [5], [6]. The state diagram is a function that relates average air velocity with air pressure drop per unit length of a pipeline having a constant inner diameter [5], [7]. The pressure drop directly relates to the air velocity in dilute phase flow operation and shifts to an indirect relationship for dense phase flow. The air velocity at the centre of this shifting curve is the optimal conveying condition, known as minimum conveying air velocity (MCAV). While the pressure drop line connecting the MCAV at different solid mass flow rates is known as the pressure drop minimum curve (PMC).

The recurring dynamics in an attractor can be visually observed in the recurrence plot (RP) initially introduced by Eckmann *et al.* [8], and its morphology is quantified using the recurrence quantification analysis [9], such as the recurrence rate, determinism and laminarity. The recurrence quantification analysis quantifies structural complexity using numbers and durations of recurring dynamics in a recurrence plot (RP). The RP represents the

dynamic topology of an attractor, developed as a visualisation tool that projects recurring dynamics from high dimensional phase space into a 2D black and white (binary values) plot [10]. It reflects the process of having trajectory points in phase space arbitrarily visiting each other at different times. RPs can reveal valuable qualitative information about the dynamic structure of attractors. Inspecting the recurrent points structure in RPs to detect slight variations in the dynamics is challenging, especially when there are multiscale recurrent structures. Moreover, The complex dynamics of gas-solid flow in fluidised bed systems have been extensively studied using RQA measures such as recurrence rate (RR) [11]–[13] to monitor and identify operating conditions where the transition between different flow patterns occurs. However, RQA has not been applied to gas-solid flow patterns in horizontal pneumatic conveying systems to quantify its complex dynamics.

This paper aims to develop the AE and RR measures from electrostatic sensor signals to characterise the unpredictability and recurring dynamics of gas-solid flow patterns behaviour in a horizontal pipeline system. The AE and RR measures are correlated with the identified flow patterns at different operating points in the state diagram. The parameters used in developing the phase space and recurrence plot are estimated using a heuristic procedure or set to a constant. The AE and RR measures are calculated from a moving window of time-series data with a fixed step, allowing the gas-solid flow patterns to be monitored and classified in real-time.

2. EXPERIMENTAL SETUP

Experimental tests have been conducted in a close-loop industrial-scale pneumatic conveying system to capture fully developed gas-solid flow behaviour in a horizontal pipeline. Figure 1 shows a schematic of the industrial-scale pneumatic conveying system and its main components. The main components of the pneumatic conveying system consist of a 0.1 m inner diameter pipeline with a total length of 127 m, receiving hopper and blow tank with a 1.5 m^3, a screw feeder, and a nozzle bank. In the loop, there are eight bends and two vertical pipeline sections. The loop consists of horizontal pipeline sections except for the sections before the second bend and after the last bend. Two screw-type compressors are used to compress air in tanks at 5.2 bar, which is then regulated and introduced in the pipeline cycle from the blow tank to receiving hopper using the nozzle bank at two locations: the blow tank exit, also known as 'blow tank air' (the screw feeder inlet), and the pipeline inlet also known as 'supplementary air' (the screw feeder outlet). The blow tank and supplementary air ratio can be adjusted per the requirement. Particulate materials are first fed to the blow tank through the feed hopper, then the blow tank is pressurised, and material is fed to the pipeline through a screw feeder using the blow tank and supplementary airflow. The air is separated from solids at the receiving hopper through a bag filter house with a surface area of 35 m^2.

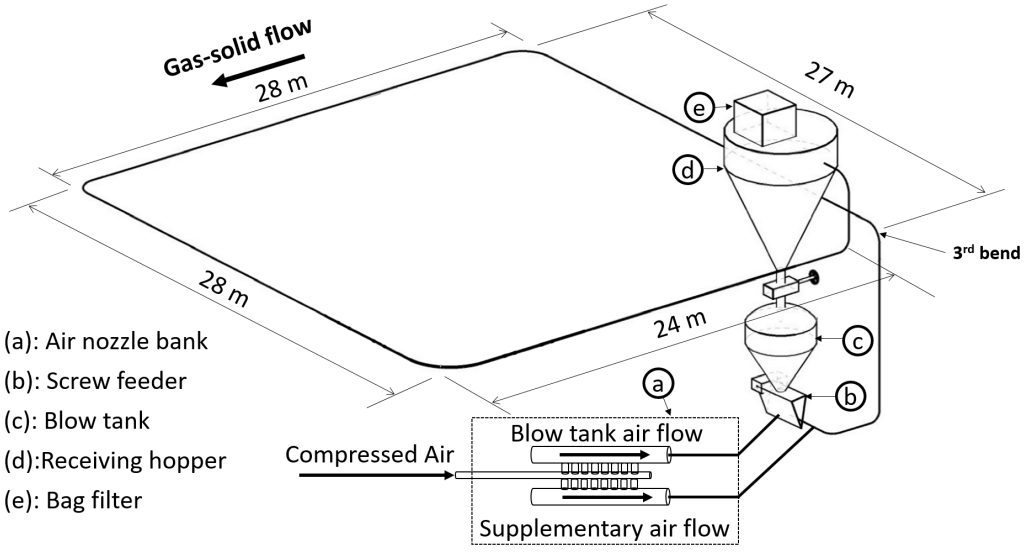

Figure 1 A schematic of the pneumatic conveying system setup used to study the fully developed gas-solid flows in the horizontal pipeline downstream of the third bend.

The solid mass flow rate is measured using a load cell at the receiving hopper and controlled by choosing a suitable air ratio between the blow tank and supplementary air and screw feeder motor speed. The air mass flow rate at the

inlet of the pneumatic conveying pipeline system is controlled using the nozzle bank. The nozzle bank consists of two sets of eight nozzle sizes, which can incrementally control the air mass flow rate at the blow tank exit and pipeline inlet using different combinations of nozzles for each set, each with a maximum limit of 0.38 kg/s.

Pressure measurements of gas-solid flow are undertaken using eight pressure transducers manufactured by DRUCK, with measurements ranging from 0 to 40kPa. Pressure sensors are installed 8 m downstream of the third bend to ensure gas-solid flow is transitioned from accelerating to fully developed. The first set of four pressure sensors is installed equidistantly with a 2m separation distance, while the second set of four pressure sensors is installed 4m after the fourth sensor with an equidistance of 2m. Kumar *et al.* [14] developed the top and bottom arc-shaped electrostatic sensors assembly to measure the average velocity of charged particles. The primary source of electrostatic charge carried around solid particles is the collisional friction between particles and the surrounding pipeline inner wall, which continuously goes through positive and negative charges with a bimodal distribution. If fully charged particles pass through the 100% sensitivity zone (bottom section of the pipeline cross-section), the voltage signal will have high magnitudes and then return to zero and vice versa. The arc-shaped electrostatic sensors assembly is placed at 0.62 m from the first pressure sensor (P1), followed by a transparent pipeline to capture flow patterns using a high-speed video camera capturing images at 240 fps, as shown in Figure 2.

Electrostatic signals were acquired from the bottom arc-shaped electrostatic electrode, which is amplified first using a transimpedance amplifier circuit with a measurement range from -5 to +5 volts and then sampled with the first pressure sensor (P1) using the National Instrument USB 6211 module at a frequency of 525 Hz. The Load cell and the rest of the pressure sensors from P2 to P8 are sampled at 1 Hz using National Instrument 6208 module, which is sufficient for state diagram representation. LabVIEW software is used to acquire data from the National Instrument modules, while the data analysis calculations are developed in MATLAB software.

A 2D grid of operating parameters is considered, including solids mass flow rate and air mass flow rate, to study gas-solid flow patterns behaviour of plastic pellets and their effect on pressure signal and bottom arc-shaped electrostatic signal. Cubical shape plastic pellets with a total batch mass of 800 kg are used, having a mean diameter of 3.6 mm, particle density of 910 kg/m^3 and bulk density of 560 kg/m^3. The air mass flow rate injected into the blow tank was kept constant throughout the transport process, and the screw feeder speed was set to five different incremental values. The solids mass flow rate is calculated using a linear regression fit of the measured solid mass time-series signal in the fully developed flow region. The average pressure values from pressure sensors P1 to P8 are used to calculate the average pressure drop through a single regression fit across the eight sensors.

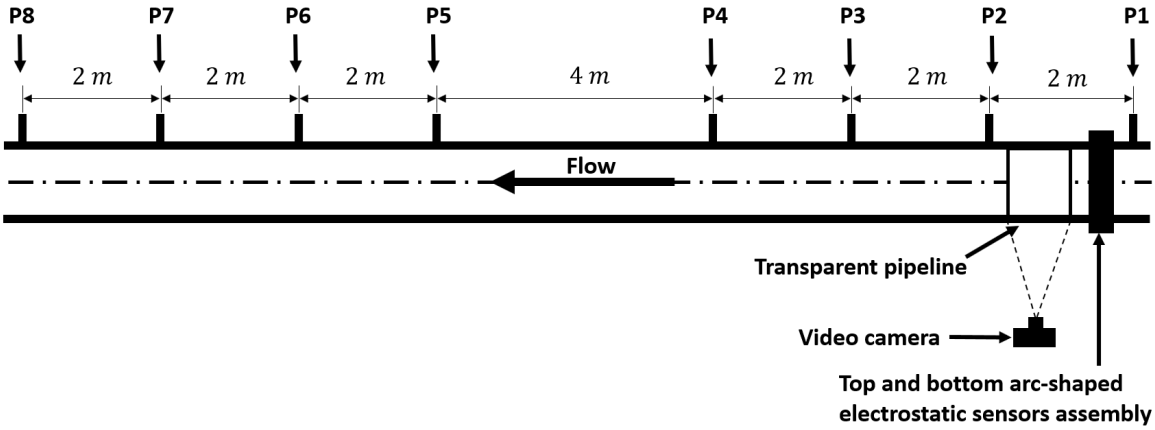

Figure 2 A schematic diagram of the horizontal pipeline downstream of the third bend showing eight pressure sensors location from P1 to P8 and the top and bottom arc-shapes electrostatic sensors assembly.

The initial experimental test point at constant screw feeder speed was conducted at a high supplementary air mass flow rate (0.4 kg/s) at the inlet of the transport pipeline to transport plastic pellets through dilute phase flow operation. Then the following test points were measured at the same screw feeder speed, and the supplementary air mass flow rate was progressively decreased by 0.02 kg/s using the nozzle bank until a single slug flow or settled layer appeared in the transparent pipeline. According to plug flow type capable materials, unstable flow in the form of slugs exists at an air velocity below the MCAV [5]. Therefore, further experiments are conducted at a constant solids mass flow rate and progressively decreasing the air mass flow rate for each test to ensure that the transition flow spectrum between dilute and dense phase flow is captured using the installed sensors to identify the MCAV.

3. ANALYSIS METHOD

3.1 Phase Space

Through time-delay coordinate embedding, one can reinflate a state variable from time-series measurements into a vector of latent state variables under the assumption that the underlying dynamic is smooth with low-dimensional manifolds [15]. This method reconstructs a phase space from a time-series signal that exhibits topological equivalence to the original system state space. Reconstructing a phase space using the time-delay coordinate embedding method from measurements requires two main parameters - time delay and embedding dimension. Consider a signal $X(t) = (x(t_1) \dots x(t_n))$, where n is the number of points acquired at constant sampling periods. Equation 1 shows the phase space data is in the form of a vector $Y(t)$ represented in the matrix form, where m is the embedding dimension, τ is the time delay, and N is the number of points in phase space ($N = n - (m-1)\tau$).

$$Y(t) = \begin{bmatrix} x(t_1) & x(t_{1+\tau}) & x(t_{1+2\tau}) & \cdots & x(t_{1+(m-1)\tau}) \\ x(t_2) & x(t_{2+\tau}) & x(t_{2+2\tau}) & \cdots & x(t_{2+(m-1)\tau}) \\ \vdots & \vdots & \vdots & \ddots & \vdots \\ x(t_N) & x(t_{N+\tau}) & x(t_{N+2\tau}) & \cdots & x(t_{N+(m-1)\tau}) \end{bmatrix} \quad (1)$$

When the dynamic complexity of a time series signal is generated from a stochastic dynamical system, its reconstructed attractor will correspond to infinite-dimensional space with no meaningful information. The false nearest neighbour algorithm (FNN) is a commonly used algorithm to estimate the embedding dimension of a signal, which is based on the idea that if not enough dimension is used to unfold the dynamics, there will be trajectory crossings in the dynamics [16]. These crossings are noise caused by high to low-dimensional space projection. This algorithm scans for trajectory crossings by distinguishing true neighbouring points from false ones for an attractor while increasing the embedding dimension.

3.2 Approximate Entropy

Approximate entropy (AE) reflects the logarithmic probability of the degree of unpredictability of future information based on previous similar information. The AE has a self-counting feature that compares the closeness of trajectory points in an attractor with other older points of itself. Zero AE corresponds to constant or cyclic behaviour, represented in phase space by a fixed point or periodic attractor. Pincus developed the approximate entropy measure, a modification of Kolmogrov-sini entropy, featured by its low computational cost and capability to deal with noisy data [17]. AE is calculated by subtracting two statistical functions; Φ_m from Φ_{m+1}, as shown in Equations 6 and 7, computed using a phase space reconstructed with the selected dimension m and at a higher dimension $m + 1$.

$$\mathrm{AE} = \Phi_m - \Phi_{m+1} \quad (2)$$

$$\Phi_m = \frac{1}{N}\sum_{i=1}^{N} log\left(\sum_{j=1, j\neq i}^{N} \Theta\left(r - \left\|Y_i - Y_j\right\|\right)\right) \quad (3)$$

3.3 Recurrence Plot and Recurrence rate

The RP is represented in a square matrix ($RP_{i,j}$) relating pairs of times at which phase points meet in a fixed hypersphere with radius r. The subscripts i and j are the indexes of the matrix for each pair of phase points. The distribution of recurrent points in an RP heavily depends on the selected threshold r. However, the r threshold selection is less critical for comparative studies of dynamical transitions, as differences between RP would not change within a specific distance range.

$$RP_{i,j} = \Theta\left(r - \left\|Y_i - Y_j\right\|\right) \quad (4)$$

The RR measure is the ratio of recurrent points to the total number of points, as shown in Equation 9.

$$RR = \frac{1}{N^2}\sum_{i=1}^{N}\sum_{j=1}^{N} RP_{i,j} \quad (5)$$

4. RESULTS AND DISCUSSIONS

4.1 Flow Pattern Map and State Diagram

The flow pattern map illustrates the formation of gas-solid flow patterns at different operating conditions. It is a scatter of operating points, including solids mass flow rate and air mass flow rate, classified into regions identified based on the flow pattern observed in a transparent pipeline. Tsuji studied the wall pressure fluctuation of horizontal gas-solid flows of plastic pellets with a mean diameter of 2.3 mm and observed its flow patterns close to the PMC, describing them as sliding dense clusters [18]. Cabrejos provided more generalised descriptions of horizontal gas-solid flow patterns and their relations to the operating conditions using three materials with different material properties [19]. The flow patterns identified for plastic pellets with a mean diameter of 3 mm are homogenous flow, stratified flow, pulsating flow, moving dunes and blowing dunes. Figure 3 shows the flow pattern map for horizontal pneumatic conveying of plastic pellets with a mean diameter of 3 mm classified into three patterns: stratified/pulsating flow, moving dunes and blowing dunes. The regions of these flow patterns vary across different gas and solids mass flow rates. Beyond the left boundary, slug flow (region D) and settled layer (region E) are present in the upper and lower regions.

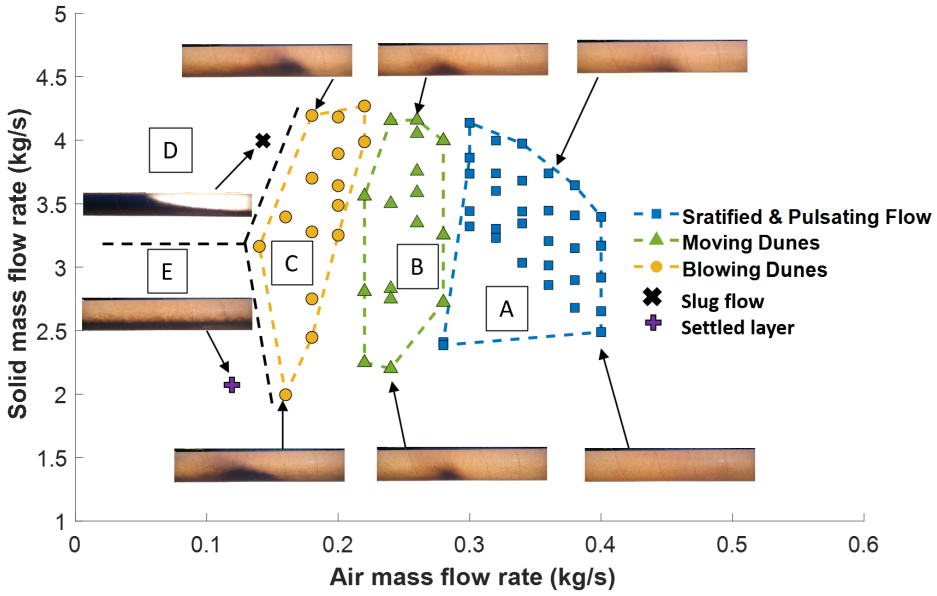

Figure 3 The flow pattern map for horizontal pneumatic conveying of plastic pellets

At a high air mass flow rate of 0.4 kg/s and low solids mass flow rate of 2.48 kg/s (lower boundary of region A), plastic pellets are in suspension mode, where particles are distributed across the pipeline cross-section with high solids concentration at the lower section of the pipeline, namely stratified flow. At the same air mass flow rate but higher solids mass flow rate of 3.6 kg/s (lower to the upper boundary in region A), plastic pellets are in an intense kinetic and frictional collision as they accumulate and form discontinuous clouds at the bottom of the pipeline, known as pulsating flow. As the air mass flow rate reduces (transition from region A to B) at a particular point, which is 0.28 kg/s in this case, self-organised critical states appear as moving dunes surrounded by dilute phase sliding on the bottom of the pipe. Moving dunes are featured by continuous erosion at the up-wind side (luff) and deposition at the down-wind side (lee). With further reduction in air mass flow rate, solid particles in dilute phase flow start to drop out of suspension, and multiple moving dunes slow down and merge, forming blowing dunes. At the left boundary of blowing dunes, dunes start to settle down, and the transportation mechanism starts to be dominated by saltation and surface creep. Beyond this boundary, plug flow (region (E)) and settled layer (region (D)) at the upper and lower regions are present.

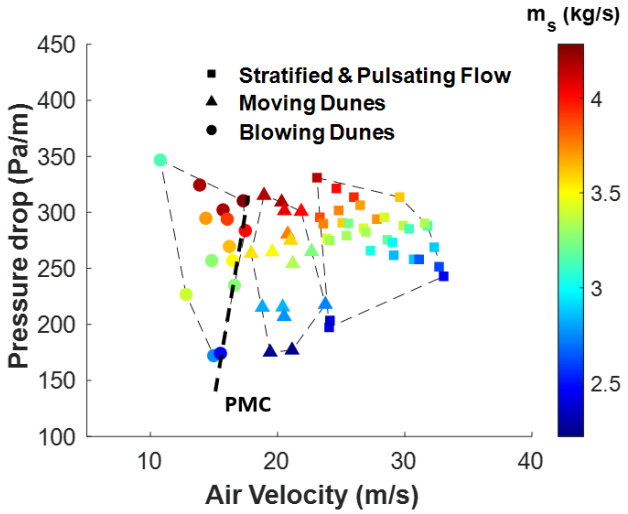

Figure 4 State diagram of plastic pellets with classified flow pattern regions

Coarse solid particles like plastic pellets with a mean diameter greater than 1 mm are expected to be conveyed at the MCAV without blockages [20]. Figure 4 shows a state diagram developed using the data gathered from the horizontal pneumatic conveying of the plastic pellets with a mean diameter of 3.6 mm. The operating points considered in developing the state diagram are the same as in the flow-pattern map presented in Figure 3. Each solid flow rate value is included for each point through a colour spectrum referring to the colour bar of values, and the flow patterns are classified into regions. The superficial air velocity is calculated based on the mean pressure and pipe diameter using the ideal gas law at ambient temperature and plotted as a function of the pressure drop per unit length of pipe. Correlating the superficial air velocity and pipeline pressure drop with gas-solid flow patterns show how specific flow patterns influence the pressure drop. The superficial air velocity in stratified, pulsating and moving dunes directly relates to the pressure drop. While the superficial air velocity of blowing dunes has an indirect relationship with the pressure drop, indicating that the PMC is between moving dunes and blowing dunes.

4.2 Analysis Parameters Settings

The approximate entropy (AE) and recurrence rate (RR) measures are calculated to a moving time window of phase spaces and recurrence plots, developed from the bottom arc-shaped electrostatic sensor data to monitor the flow at different operating conditions. The parameters required to reconstruct a moving phase space window are moving time window size and step, embedding dimension and time delay. The AE measure is calculated from the reconstructed phase spaces using a threshold radius ($r_{AE\ Max}$), while the RR measure is calculated from recurrence plots developed from the reconstructed phase spaces using a threshold radius (r_{RP}).

The moving window size is set to 5s of data and the window step to 1s. The phase spaces are reconstructed using a time delay of 1, and the embedding dimension is estimated using FNN. The embedding dimensions are estimated for the electrostatic sensor data acquired at the operating points in Figure 1, which vary between 9 and 13. The choice of dimension used to reconstruct the moving phase spaces window at all operating conditions is set to a constant of 10. The threshold r_{RP} is selected based on the approximate entropy (AE) distribution of the phase spaces across different thresholds r.

AE is the probability that future similar trajectories, including stochastic and deterministic, do not follow past similar trajectories. The chance that trajectory points in an attractor have other points than itself falling within a hypersphere with a small r is zero or very low. As r increases, more trajectory points are included in determining the probability between future and past similar dynamics. A typical distribution of AE across r is an increase in the unpredictability of information up to a specific r, forming the most significant difference between past and future information, as shown in Figure 3. The distribution of AE beyond this particular r gradually decreases to zero as the relation between future information becomes regular to the past information, and r approaches the maximum value between the points. It is recommended to select r within the range of 0.1 to 0.2 times the standard deviation of the signal. Sometimes the standard deviation approach may lead to an incorrect assessment of the signal complexity [21]. A more appropriate approach is to select the maximum value of AE (AE_{max}) across r or an

AE at a slightly higher r than the r at AE_{max} (r_{AEmax}) to avoid misleading comparative results [22]. The AE values shown in Figure 3 are calculated at 50 equidistant r across the phase spaces reconstructed from electrostatic signals to identify r_{AEmax} and select AE_{max}.

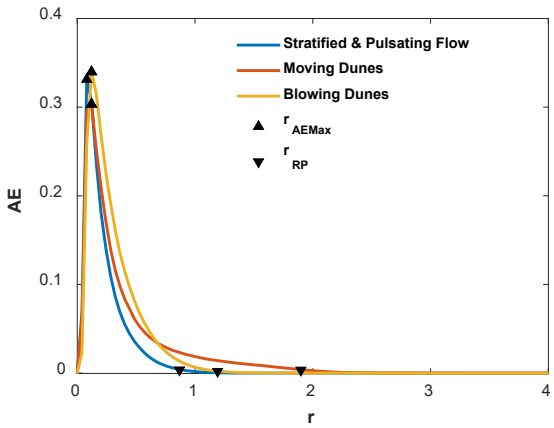

Figure 5 An approximate entropy vs radius of bottom arc-shaped electrostatic sensor signals acquired at air velocities 33.5, 20 and 16 m/s and ms = 2.6, 2.2 and 2.5 kg/s representing the stratified flow, moving dunes and blowing dunes

Extracting meaningful measures from RPs requires an appropriate threshold r_{RP}, typically depending on the application type [23]. Initial rules of thumb choices for r_{RP} are taken at 10% of the maximum diameter of phase space or 5% of the mean diameter [9] or a threshold r at a 1% recurrence rate [24]. Using the recurrent diagonal structures parallel to the LOI in RPs was appropriate for optimal threshold selection for quasiperiodic systems [25]. Later Gao and Jin [26] presented a criterion for selecting the optimum threshold using the first maximum value of the derivative of the recurrence rate with respect to the r (dRR/dr). However, the r at the first maximum value of dRR/dr can be impractical when there are multiple maxima across r, clearly observed in quasiperiodic systems [27]. Instead of looking at the dRR/dr to select the threshold r_{RP}, AE is used to have more consistent RR measures. The r_{RP} threshold is selected at a decreasing AE across r to ensure that the RPs will have a high probability of predictable dynamics, specifically at the centre between r_{AEmax} and zero AE, shown in Figure 3.

Figures 4 (a) and (b) show the AE and RR time-series signals developed from the bottom arc-shaped electrostatic sensor data using the parameter setting mentioned above for different flow patterns, indicating that the AE signal for moving dunes has the lowest values, while its RR signal has the highest values.

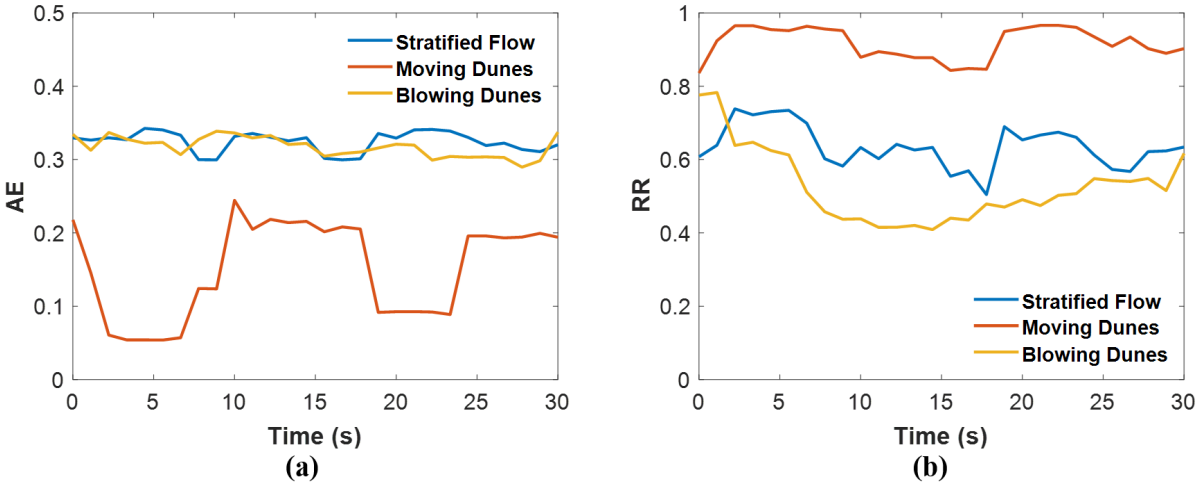

Figure 6 (a) AE signals and (b) RR signals developed from bottom arc-shaped electrostatic sensor signals acquired at air velocities of 33, 20 and 10 m/s and solid mass flow rate of 3, 3.5 and 3.1 kg/s representing the stratified flow, moving dunes and blowing dunes

4.3 Approximate Entropy of Electrostatic Sensor Signals

Figure 5 shows the profile of the average AE signals over the 30s of electrostatic sensor data across the operating points in the state diagram, expressing the relationship between the unpredictability of electrostatic sensor signals and classified flow patterns. The profile of AE in the stratified and pulsating flow have relatively similar values, ranging between 0.26 and 0.33, indicating that the concentration of individual charged particles at the bottom of the pipeline in the stratified and pulsating flow have similarity in their unpredictability. The AE decreases below 0.26 in the moving dunes region, having the lowest values, ranging between 0.17 and 0.26, at the MCAV, which is at the transition between moving dunes and blowing dunes. Before the flow transition to slug flow and stratified layer from the blowing dunes region, the AE increases rapidly to 0.3, reflecting a sudden change in the unpredictability of the flow.

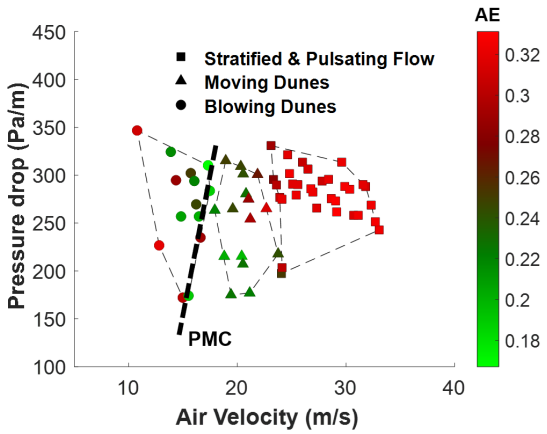

Figure 7 State diagram correlated with approximate entropy of bottom arc-shaped electrostatic sensor signals

4.4 Recurrence Plot of Electrostatic Sensor Signals

Figure 6 shows the 2s of bottom arc-shaped electrostatic sensor signals and their recurrence plots (RPs) for three flow patterns, stratified flow, the moving dunes and near the blowing dunes transition to the settled layer. The solids concentrations of charged particles and their arrangement across the pipeline bottom cross-section for each flow pattern have different effects on the voltage signal from the bottom arc-shaped electrostatic sensor. These voltage signals are directly related to the charging capacity of particles and their location in the local sensitivity region of the sensor. The evolution of electrostatic signals from the stratified flow to blowing dunes shows an increase in the short-term peaks, represented in the recurrence plots as vertical white bands, which can be directly related to the sudden increase in electrostatic activity of dunes having high solid concentrations.

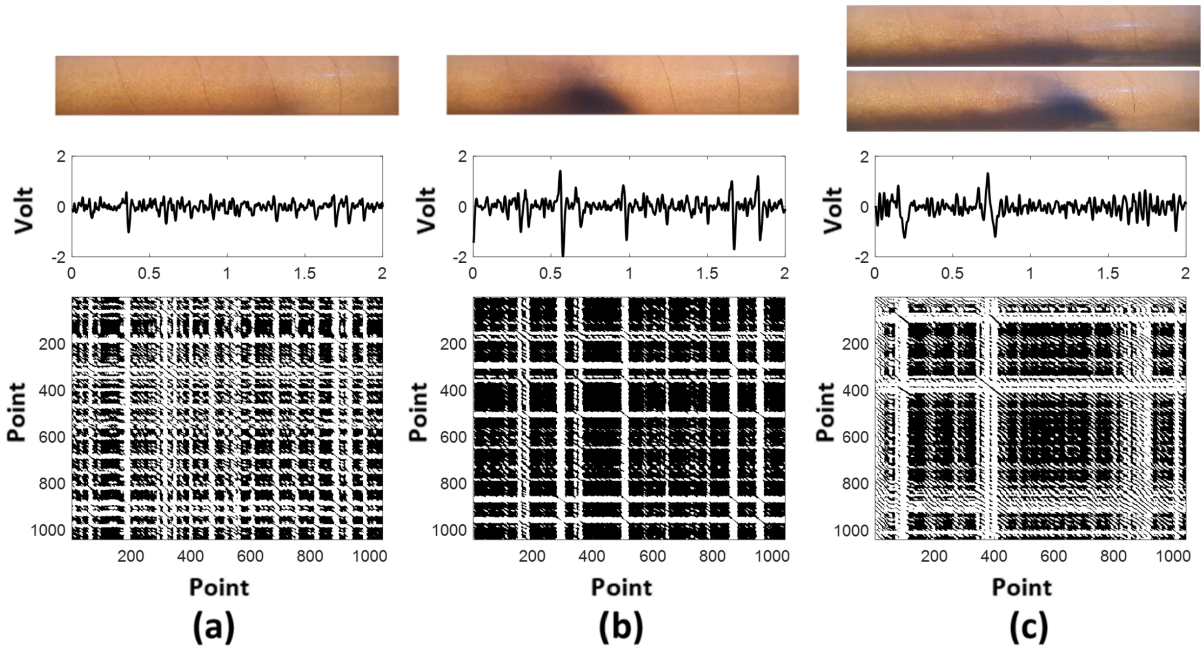

Figure 8 Bottom arc-shaped electrostatic signals and their recurrence plots for (a) stratified flow, (b) moving dunes and (c) blowing dunes transitioning to settling layer at air velocities 33.5, 20 and 16 m/s and m_s = 2.6, 2.2 and 2.5 kg/s.

4.5 Recurrence Quantification Analysis Measures

Figure 7 shows the profile of the average RR signals over the 30s of electrostatic sensor data across the operating points in the state diagram. The RR values have a smooth increase as the flow transitions from stratified flow at low m_s of 2.2 kg/s to pulsating flow at high m_s of 4.3 kg/s. However, the RR values at m_s of 4.3 kg/s cannot detect changes between pulsating flow and moving dunes. The transition between moving dunes and blowing dunes corresponds to the highest RR values, indicating that the electrostatic dynamics of dunes are very similar to each other at the MCAV. The RR values at the left boundary of blowing dunes suddenly drop just before slugs develop at a high solid mass flow rate or form a settled layer at low solids mass flow rate.

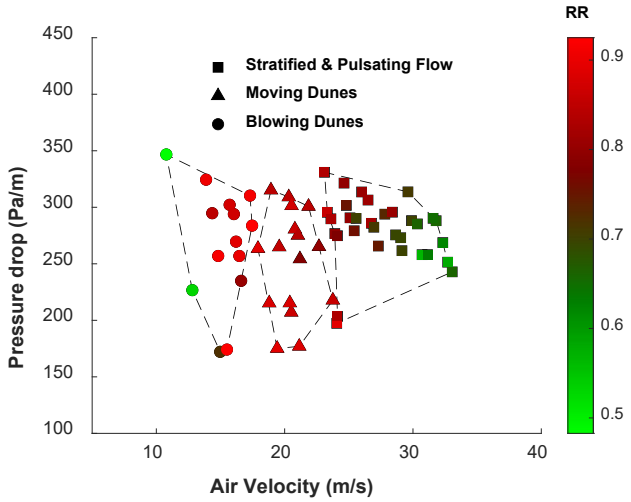

Figure 9 State diagrams for plastic pellets correlated with the RR of bottom arc-shaped electrostatic sensor signal

5. CONCLUSIONS

The approximate entropy (AE) and recurrence rate (RR) measures developed from bottom arc-shaped electrostatic signals in horizontal pneumatic conveying of plastic pellets have been successfully developed to characterise flow patterns in the transition phase between dilute and dense phase flow operations. A state diagram of plastic pellets is developed using different operating parameters, air mass flow rate and solids mass flow rate, correlated with the observed flow patterns, including stratified/pulsating flow, moving dunes, and blowing dunes. It is found that optimal conditions at minimum energy consumption operation are located between moving dunes and blowing dunes.

The AE is applied to describe the probability of unpredictable dynamics in electrostatic sensor signals and to estimate a radius threshold parameter for developing recurrence plots. The RR is then calculated from the developed recurrence plot to characterise recurring dynamics in the signals. The RPs at low solids mass flow rates ranging from 2 to 3.3 kg/s and decreasing air velocity reveal various local white areas (LWA) and local bolt areas (LBA), providing qualitative information on the effect of observed flow patterns on the electrostatic signals fluctuations. The LBA in RPs of electrostatic signals increases from stratified flow to moving dunes and decreases from moving dunes to blowing dunes transitioning to settled layer, indicating that the similarity in the dynamics of charged particles in moving dunes are high in comparison to individual charged particles in stratified flow and settling blowing dunes.

The average values of AE and RR time-series across the 30s of electrostatic sensor data at different operating parameters are correlated with the air velocity, pressure drop and observed flow patterns at various solids mass flow rates ranging from 2.2 to 4.2 kg/s. The AE time series showed that the transition between moving dunes and blowing dunes has lower AE values than stratified/pulsating flow, while RR have the highest values.

6. ACKNOWLEDGEMENTS

The author would like to acknowledge the financial support from the University of Greenwich through VC scholarship (VCS-ES-04-19) and technical support from the entire team at the Wolfson Centre for Bulk Solids Handling Technology, University of Greenwich.

7. NOMENCLATURE

MCAV	Minimum conveying air velocity, m/s
PMC	Pressure drop minimum curve, Pa/m
P1 to P8	Pressure sensor tapings
t	Time, s
x(t)	Data point value at specific t
X(t)	Time series data
τ	Time delay
m	Embedding dimension
n	Number of data points
N	Number of phase points
Y(t)	Phase space (Time series vector)
Φ	Statistical function
RP	Recurrence plot Matrix
r	Radius of a hypersphere
RR	Recurrence rate

8. REFERENCES

[1] D. Mills, *Pneumatic Conveying Design Guide*, Third edit. Butterworth-Heinemann, 2016. doi: 10.1016/C2014-0-02678-0.

[2] A. E. Kabeel, M. Elkelawy, H. A. E. D. Bastawissi, and A. M. Elbanna, "An experimental and theoretical study on particles-in-air behavior characterization at different particles loading and turbulence modulation," *Alexandria Engineering Journal*, vol. 58, no. 2, pp. 451–465, 2019, doi: 10.1016/j.aej.2019.04.002.

[3] G. Klinzing, F. Rizk, R. Marcus, and L. S. Leung, *Pneumatic Conveying of Solids: A theoretical and practial approach*, Third edit. Springer, 2010. doi: 10.1007/978-90-481-3609-4.
[4] A. Levy and H. Kalman, *Handbook of Conveying and Handling of Particulate Solids*, First edit. Elsevier, 2001.
[5] P. W. Wypych and J. Yi, "Minimum transport boundary for horizontal dense-phase pneumatic conveying of granular materials," *Powder Technol*, vol. 129, no. 1–3, pp. 111–121, 2003, doi: 10.1016/S0032-5910(02)00224-3.
[6] A. K. Saha, D. Das, R. Srivadtava, P. K. Panigrahi, and K. Muralidhar, *Fluid Mechanics and Fluid power - Contemporary Research*. 2016. doi: 10.1007/978-81-322-2743-4.
[7] A. B. Makwana, A. Patankar, and M. Bose, "Effect of dune formation on pressure drop in horizontal pneumatic conveying system," *Particulate Science and Technology*, vol. 33, no. 1, pp. 59–66, 2015, doi: 10.1080/02726351.2014.936541.
[8] J. P. Eckmann, O. Oliffson Kamphorst, and D. Ruelle, "Recurrence plots of dynamical systems," *Europhys Lett*, vol. 4, no. 9, pp. 973–977, 1987, doi: 10.1209/0295-5075/4/9/004.
[9] J. P. Zbilut and C. L. Webber Jr, "Embeddings and delays as derived from quantification of recurrence plots," *Phys Lett A*, vol. 171, no. 3–4, pp. 199–203, 1992, doi: 10.1016/0375-9601(92)90426-M.
[10] J. P. Eckmann, O. Oliffson Kamphorst, and D. Ruelle, "Recurrence plots of dynamical systems," *Europhys Lett*, vol. 4, no. 9, pp. 973–977, 1987, doi: 10.1209/0295-5075/4/9/004.
[11] B. Babaei, R. Zarghami, H. Sedighikamal, R. Sotudeh-Gharebagh, and N. Mostoufi, "Investigating the hydrodynamics of gas-solid bubbling fluidization using recurrence plot," *Advanced Powder Technology*, vol. 23, no. 3, pp. 380–386, May 2012, doi: 10.1016/j.apt.2011.05.002.
[12] M. Tahmasebpour, R. Zarghami, R. Sotudeh-Gharebagh, and N. Mostoufi, "Characterization of various structures in gas-solid fluidized beds by recurrence quantification analysis," *Particuology*, vol. 11, no. 6, pp. 647–656, 2013, doi: 10.1016/j.partic.2012.08.005.
[13] M. F. Llop and N. Gascons, "Multiresolution analysis of gas fluidization by empirical mode decomposition and recurrence quantification analysis," *International Journal of Multiphase Flow*, vol. 105, pp. 170–184, 2018, doi: 10.1016/j.ijmultiphaseflow.2018.04.006.
[14] A. Kumar, T. Deng, and M. S. A. Bradley, "Application of arc-shaped electrostatic sensors for monitoring the flow behaviour at top and bottom section of a pneumatic conveying pipeline," *Measurement: Sensors*, vol. 10–12, no. 10–12, pp. 1–8, 2020, doi: 10.1016/j.measen.2020.100026.
[15] F. Takens, "Detecting strange attractors in turbulence Dynamical Systems and Turbulence," *Dynamical Systems and Turbulence*, vol. 898, pp. 366–381, 1981.
[16] C. Rhodes and M. Morari, "The false nearest neighbors algorithm: An overview," *Comput Chem Eng*, vol. 21, pp. 1149–1154, 1997, doi: 10.1016/S0098-1354(97)87657-0.
[17] S. M. Pincus, "Approximate entropy as a measure of system complexity," *Proc Natl Acad Sci U S A*, vol. 88, no. 6, pp. 2297–2301, 1991, doi: 10.1073/pnas.88.6.2297.
[18] Y. Tsuji, Y. Morikawa, S. Sugimotc, S. I. Miyoshi, and Y. Nakano, "Flow Pattern and Pressure Fluctuation in Air-Solids Two-Phase Flow in a Pipe at Low Velocities," *International Journal of Multiphase Flow*, vol. 48, no. 428, pp. 656–663, 1982, doi: 10.1299/kikaib.48.656.
[19] F. J. Cabrejos and G. E. Klinzing, "Characterization of dilute gas-solids flows using the rescaled range analysis," *Powder Technol*, vol. 84, no. 2, pp. 139–156, 1995, doi: 10.1016/0032-5910(95)02980-G.
[20] M. G. Jones and K. C. Williams, "Predicting the mode of flow in pneumatic conveying systems-A review," *Particuology*, vol. 6, no. 5, pp. 289–300, 2008, doi: 10.1016/j.partic.2008.05.003.
[21] S. Lu, X. Chen, J. K. Kanters, I. C. Solomon, and K. H. Chon, "Automatic selection of the threshold value r for approximate entropy," *IEEE Trans Biomed Eng*, vol. 55, no. 8, pp. 1966–1972, Aug. 2008, doi: 10.1109/TBME.2008.919870.
[22] A. Delgado-Bonal and A. Marshak, "Approximate entropy and sample entropy: A comprehensive tutorial," *Entropy*, vol. 21, no. 6. MDPI AG, Jun. 01, 2019. doi: 10.3390/e21060541.
[23] N. Marwan, "How to avoid potential pitfalls in recurrence plot based data analysis," *International Journal of Bifurcation and Chaos*, vol. 21, no. 4, pp. 1003–1017, 2011, doi: 10.1142/S0218127411029008.
[24] J. P. Zbilut, J. M. Zaldivar-Comenges, and F. Strozzi, "Recurrence quantification based Liapunov exponents for monitoring divergence in experimental data," *Physics Letters, Section A: General, Atomic and Solid State Physics*, vol. 297, no. 3–4, pp. 173–181, 2002, doi: 10.1016/S0375-9601(02)00436-X.
[25] L. Matassini, H. Kantz, J. Hołyst, and R. Hegger, "Optimizing of recurrence plots for noise reduction," *Phys Rev E*, vol. 65, no. 2, pp. 1–6, 2002, doi: 10.1103/PhysRevE.65.021102.
[26] Z. Gao and N. Jin, "Flow-pattern identification and nonlinear dynamics of gas-liquid two-phase flow in complex networks," *Phys Rev E*, vol. 79, no. 6, pp. 1–14, 2009, doi: 10.1103/PhysRevE.79.066303.
[27] R. v. Donner, Y. Zou, J. F. Donges, N. Marwan, and J. Kurths, "Ambiguities in recurrence-based complex network representations of time series," *Phys Rev E Stat Nonlin Soft Matter Phys*, vol. 81, no. 1, pp. 2–6, 2010, doi: 10.1103/PhysRevE.81.015101.